nature communications

Article

https://doi.org/10.1038/s41467-025-59849-1

Targeting C1q prevents microglia-mediated synaptic removal in neuropathic pain

Received: 10 November 2021

Accepted: 7 May 2025

Published online: 17 May 2025

Check for updates

Noosha Yousefpour[1,2,3], Shannon N. Tansley[2,4,5], Samantha Locke[1,2], Behrang Sharif[2,6,7], Marc Parisien[2,8], Farin B. Bourojeni[2,9], Haley Deamond[1,2], Vidhu Mathur[3], Nia Rahman-Khan Arana[3], Jean Sebastien Austin[4], Valerie Bourassa[1,2], Chengyang Wang[4], Valérie C. Cabana[1], Calvin Wong[2,5], Kevin C. Lister[2,4,5], Rose Rodrigues[1,2,10], Manon St-Louis[1], Marie-Eve Paquet[11,12], Michael C. Carroll[13], Yaisa Andrews-Zwilling[3], Philippe Seguela[2,6], Artur Kania[2,9,10,14], Ted Yednock[3], Jeffrey S. Mogil[2,4], Yves De Koninck[2,12,15], Luda Diatchenko[2,5,8], Arkady Khoutorsky[2,5,8] & Alfredo Ribeiro-da-Silva[1,2,10] ✉

Activation of spinal microglia following peripheral nerve injury is a central component of neuropathic pain pathology. While the contributions of microglia-mediated immune and neurotrophic signalling have been well-characterized, the phagocytic and synaptic pruning roles of microglia in neuropathic pain remain less understood. Here, we show that peripheral nerve injury induces microglial engulfment of dorsal horn synapses, leading to a preferential loss of inhibitory synapses and a shift in the balance between inhibitory and excitatory synapse density. This synapse removal is dependent on the microglial complement-mediated synapse pruning pathway, as mice deficient in complement C3 and C4 do not exhibit synapse elimination. Furthermore, pharmacological inhibition of the complement protein C1q prevents dorsal horn inhibitory synapse loss and attenuates neuropathic pain. Therefore, these results demonstrate that the complement pathway promotes persistent pain hypersensitivity via microglia-mediated engulfment of dorsal horn synapses in the spinal cord, revealing C1q as a therapeutic target in neuropathic pain.

Damage or disease of the nervous system can trigger a form of pathological pain known as neuropathic pain[1]. Symptoms of this debilitating disorder include spontaneous, ongoing, or shooting pain, in addition to an amplified pain sensation in response to both noxious and innocuous stimuli[2]. It is becoming increasingly evident that activation of spinal microglia, the resident immune cells in the central nervous system, plays a crucial role in the development of neuropathic pain[3,4]. Following nerve injury, spinal microglia proliferate and undergo drastic morphological changes[5]. These changes are accompanied by an upregulation of genes associated with the reactive state of microglia, the production and release of potent immune mediators and neuromodulators, and an increase in phagocytotic activity[6–8]. Of these functions, far less is known about the role of microglial phagocytosis within the context of synapse pruning, and its implications in modulating spinal cord synaptic connectivity in neuropathic pain[9]. This is particularly important because maladaptive structural changes in the dorsal horn, such as loss of inhibitory synapses, are likely key contributing factors to the chronic nature of neuropathic pain[10,11].

During development, microglia prune synapses by employing various phagocytic signalling pathways[12]. In early postnatal life,

A full list of affiliations appears at the end of the paper. ✉e-mail: alfredo.ribeirodasilva@mcgill.ca

microglia use the classical complement pathway to identify and remove weak synapses in the visual system[13]. In this model, complement proteins C1q and C3-derived complement fragment C3b are localized to synapses that are then targeted for engulfment by microglia via complement receptor 3 (CR3). On the other hand, microglia use the fractalkine receptor, CX3CR1, to regulate dendritic spine formation on hippocampal neurons[14]. Signaling between CX3CR1, and its ligand, neuronal CX3CL1, results in the elimination of weak synapses. Interestingly, these pathways are reactivated in several neurological disorders in adults[15–17]. In animal models of neuropathic pain, microglial surface receptors CR3 and CX3CR1 are upregulated in the spinal cord, suggesting that these pruning pathways might play a role in the pathology of pain[18,19]. However, whether they directly contribute to the sensory symptoms of neuropathic pain remains unknown.

Here, we used a preclinical model of neuropathic pain to investigate engulfment of synaptic elements in combination with changes to synapse numbers in the dorsal spinal cord. We demonstrated that while nerve injury-activated microglia engulf both spinal inhibitory and excitatory terminals, there is a marked loss of inhibitory, but not excitatory synapses. Furthermore, we found that either global depletion of microglia, genetic deletion of complement C3 or C4, as well as pharmacological inhibition of C1q, all fully protect against inhibitory synapse loss and unmask the dynamics of excitatory synapse changes. Therefore, we conclude that the complement pathway mediates synapse elimination in the dorsal horn of the spinal cord following nerve injury. Importantly, pharmacological inhibition of C1q alleviated mechanical hypersensitivity. Together, these results uncover a previously unrecognized role of complement-mediated synapse pruning in neuropathic pain and reveal that targeting C1q is a disease-modifying strategy to prevent maladaptive dorsal horn synaptic reorganization following peripheral nerve injury.

Results

Nerve injury triggers engulfment of presynaptic terminals by microglia

We first assessed the phagocytic capacity of spinal microglia to engulf inhibitory and excitatory neuronal structures at different time points after peripheral nerve injury. Mice were subjected to spared nerve injury (SNI), and engulfment of neuronal structures by dorsal horn microglia was quantified at day 3, 7, 14, and 21 post-SNI. To identify and differentiate inhibitory and excitatory neuronal structures, we used mice expressing tdTomato fluorescent protein in inhibitory neurons ($Gad2^{Cre}$; tdTomato, referred to as Gad2-tdTom, Fig. 1a1), substance P-expressing excitatory neurons ($Tac1^{Cre}$; tdTomato, referred to as Tac1-tdTom, Fig. 1b1), all dorsal horn excitatory neurons ($Lmx1b^{Cre}$; tdTomato, referred to as Lmx1b-tdTom, Supplementary Fig. 1a1), and a major sub-set of lamina II primary afferents ($MrgD^{Cre}$; tdTomato referred to as MrgD-tdTom). Substance P is expressed in a subset of excitatory spinal interneurons and primary afferents that are implicated in nociceptive transmission[20]. We focused our analysis on lamina II of the spinal dorsal horn where neuronal circuits that are critical for sensory information processing exist[21]. To quantify engulfment of genetically labeled inhibitory and excitatory neuronal structures, high-resolution three-dimensional stacks of dorsal horn microglia were analyzed for the presence of neuronal-derived $tdTomato^+$ elements within microglial $CD68^+$ lysosomes (Figs. 1a2-5, 1b2-5, Supplementary Figs. 1a2-5 and 1b1-2). Notably, a significant increase in the total volume of inhibitory and excitatory neuronal structures within lysosomes of ipsilateral microglia was observed at day 7 post-SNI, but not at day 3 (Gad2-tdTom: $t_{88} = 9.6$, $p < 0.0001$; Tac1-tdTom: $t_{88} = 7.4$, $p < 0.0001$) (Figs. 1a6 and 1b6). This phagocytic activity of microglia peaked at 7 days after injury and remained elevated for the following two weeks (Gad2-tdTom: $t_{88} = 3.7$, $P = 0.0012$; Tac1-tdTom: $t_{88} = 3.3$, $p = 0.0043$). At day 7 post-injury, engulfment of excitatory structures in Tac1-tdTom mice was comparable to that observed in Lmx1b-tdTom mice, and no significant engulfment of $MrgD^+$ primary afferent inputs was detected (Supplementary Figs. 1a6 and 1b3). Temporal analyses showed no significant difference in the time course of engulfment of inhibitory and excitatory structures, however, a greater volume of inhibitory as compared to excitatory elements was engulfed at day 7 post-SNI ($t_{22} = 1.3$, $P < 0.0001$) (Figs. 1a6, 1b6 and Supplementary Figs. 1a6-7, 1c1, and 1c2).

To further study which sub-cellular components of dorsal horn neurons were engulfed by microglia, we performed immunocolocalization analyses of CD68 and markers of different neuronal compartments within Iba1-labeled microglia. To assess the engulfment of synaptic terminals from inhibitory and excitatory interneurons, we used immunohistochemistry to detect synapse-specific proteins, VGAT and VGLUT2, respectively[22] (Figs. 1c1-2 and 1d1-2). Quantifications of specific synaptic markers showed a similar trend to engulfment of neuronal elements (Figs. 1c3 and 1d3). At day 7 post-injury, there was a two-fold increase in the total volume of $VGAT^+$ and $VGLUT2^+$ terminals within microglial lysosomes sampled from the ipsilateral dorsal horn as compared to the contralateral side (VGAT: $t_{88} = 8.5$, $P < 0.0001$; VGLUT2: $t_{88} = 4.7$, $P < 0.0001$) (Figs. 1c3 and 1d3). Consistent with our previous results, we detected an increase in engulfment at days 14 and 21 post-SNI for both synaptic markers (Figs. 1c3 and 1d3).

To determine whether other neuronal structures were engulfed by microglia, we examined the engulfment of neuronal marker, NeuN, which labels nuclei and cytoplasm[23,24], as well as inhibitory (gephyrin) and excitatory (homer1) postsynaptic and intracellular proteins, and found no evidence of their engulfment at 3, 7, 14, and 21 days post-SNI (Supplementary Figs. 1d1-3). We found no change in the number of dorsal horn inhibitory ($Gad2^+$) and excitatory ($Tac1^+$) neurons at day 21 post-injury, indicating that the increase in engulfment of presynaptic elements was not caused by neuronal loss (Supplementary Fig. 1e). Thus, both inhibitory and excitatory presynaptic terminals are engulfed by nerve injury-activated microglia in the dorsal horn of neuropathic mice.

Transient depletion of microglia attenuates mechanical hypersensitivity and prevents dorsal horn synapse loss

It is well established that microglia play an important role in neuropathic pain pathology[25] as targeting of microglia has been shown to prevent and reverse pain behavior in models of neuropathic pain[4,7]. To study the contribution of microglia-mediated synaptic engulfment to neuropathic pain, we transiently depleted microglia during the peak of their engulfment activity, determined based on the temporal analysis of synapse engulfment (Fig. 1c3 and 1d3). To this end, we pharmacologically blocked microglial survival signaling, using PLX3397 (a colony stimulating factor 1 receptor inhibitor), for 6 consecutive days starting from day 5 post-injury (Fig. 2a). Daily intraperitoneal treatments of PLX3397 depleted 91% of dorsal horn microglia and eliminated the nerve injury-induced difference in microglial count between ipsilateral and contralateral dorsal horn by the end of the treatment period on day 10 post-SNI (vehicle: $t_{40} = 9.2$, $P < 0.0001$; PLX3397: $t_{40} = 0.2$, $P > 0.9999$) (Fig. 2b, c). Within 10 days following the end of treatment, microglia repopulated the dorsal horn with a greater number of cells in the ipsilateral side as compared to the contralateral side (vehicle: $t_{40} = 8.9$, $P < 0.0001$; PLX3397: $t_{40} = 3.6$, $P = 0.0026$) (Fig. 2b, c). Next, we assessed the effect of transient depletion of microglia on mouse pain behavior. We observed a reduction in mechanical hypersensitivity at all time points following SNI in PLX3397-treated mice as compared to vehicle-treated mice (treatment × repeated measures: $F_{3120} = 25.8$, $p < 0.0001$; time: F_{1120}: 25.8, $P < 0.0001$) (Fig. 2d). Although the analgesic effect of transient microglial depletion was greater during the depletion period, some analgesia was still detectable when microglia repopulated the spinal cord. Microglia gradually recovered

https://doi.org/10.1038/s41467-025-59849-1

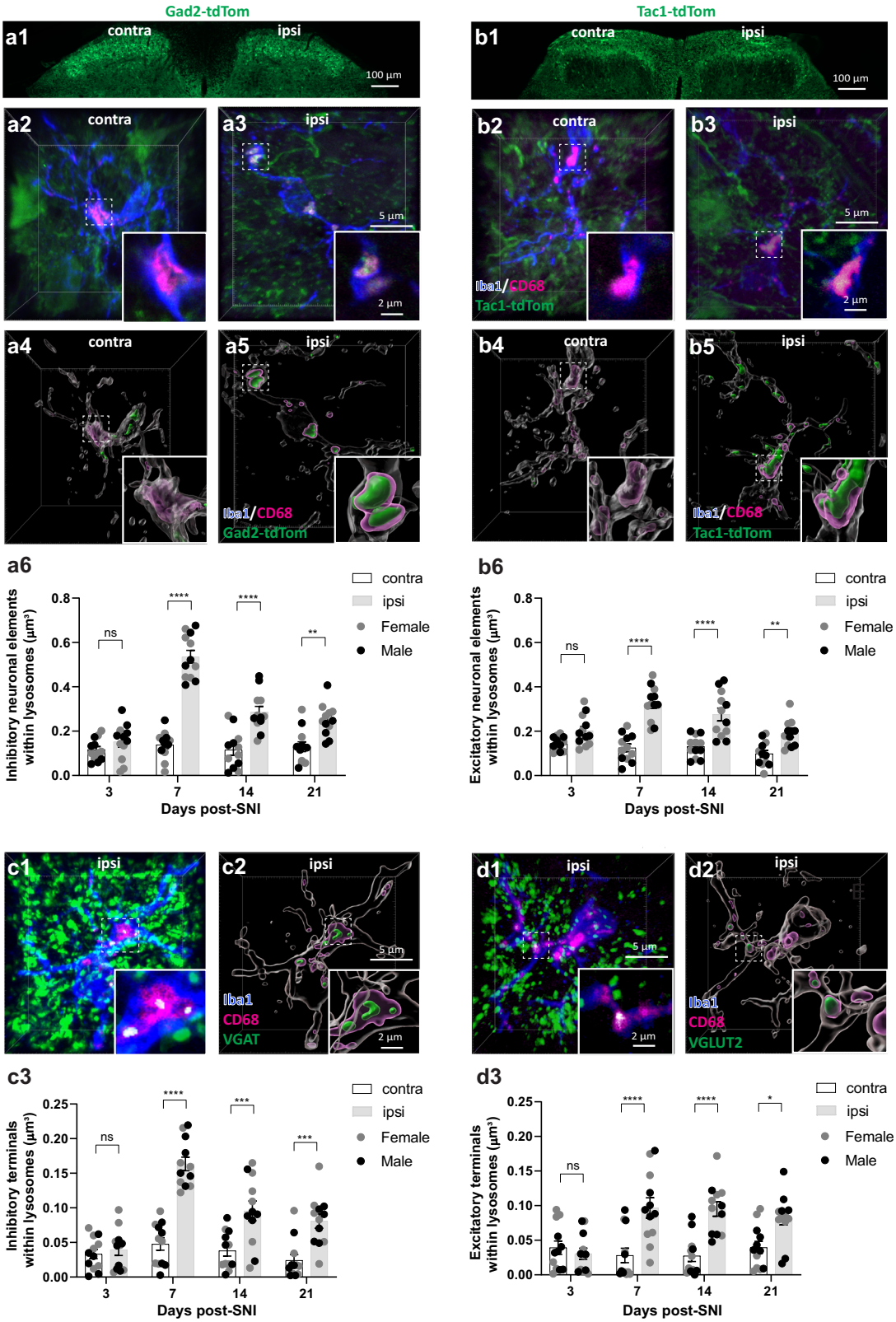

their synapse engulfment capacity within the next 10 days following the end of treatment (Fig. 2e, f).

To determine whether nerve injury induces synapse loss and if this loss is caused by microglia-mediated engulfment of presynaptic terminals, dorsal horn inhibitory and excitatory synapse densities were quantified in neuropathic mice using structured illumination microscopy (SIM). For inhibitory synapses, presynaptic terminals were labeled with antibodies against VGAT, and postsynaptic sites were labeled with an anti-gephyrin antibody. A synapse was counted when VGAT and gephyrin immunoreactive puncta were in close apposition (Fig. 2g). Consistent with previous reports[11], peripheral nerve injury resulted in a 27% reduction in the number of lamina II inhibitory synapses quantified as density of VGAT and gephyrin pairs (vehicle: $t_{96} = 4.0$, $P = 0.0002$) (Fig. 2i). Notably, depletion of microglia

Fig. 1 | Nerve injury triggers engulfment of presynaptic terminals by microglia. **a1, b1** Expression of tdTomato fluorescent protein reporter in the dorsal horn of Gad2-tdTom (**a1**) and Tac1-tdTom (**b1**) mice to demonstrate the distributions of inhibitory Gad65-expressing and excitatory substance P-expressing neurons, respectively. **a2-5-b2-5** Representative 3D reconstructions (**a2-3, b2-3**) and surface rendering (**a4-5, b4-5**) of microglia (blue) sampled from dorsal horn (lamina II) to show internalized inhibitory and excitatory neuronal elements (green) within lysosomal compartments (magenta) of ipsilateral microglia. Insets within raw images are single plane enlarged images selected from confocal stacks illustrating the presence of tdTomato fluorescent signals inside lysosomes. Insets within 3D reconstructions are enlarged views of the engulfed volumes from the same regions. **a6, b6** Quantifications of temporal changes of engulfment of inhibitory (**a6**) and excitatory (**b6**) tdTomato$^+$ neuronal elements by microglia ($n = 12$ mice per group; 6 mice per sex). **c1, d1** Three-dimensional fluorescent images of microglia (blue) sampled from ipsilateral dorsal horn labeled for lysosomal marker CD68 (magenta), marker of presynaptic inhibitory terminals (VGAT; green) (**c1**) and marker of presynaptic excitatory terminals (VGLUT2; green) (**d1**). Representative 3D surface-rendered images illustrate the engulfment of presynaptic elements (**c2, d2**). **c3-d3** Quantifications of temporal changes of engulfment of inhibitory (**c3**) and excitatory (**d3**) presynaptic terminals by microglia ($n = 12$ mice per group; 6 mice per sex. Means are plotted with individual data points ± SEM. $^*p < 0.05$, $^{**}p < 0.01$, $^{***}P < 0.001$, and $^{****}P < 0.0001$ analyzed with two-way ANOVA followed by Bonferroni post hoc test. Source data are provided as a Source Data file.

prevented loss of inhibitory synapses in the ipsilateral dorsal horn without affecting the contralateral dorsal horn synapse density (PLX3397: $t_{96} = 0.3$, $P > 0.9999$) (Fig. 2i). To assess excitatory synapse density, presynaptic terminals were labeled with anti-VGLUT2 antibody and postsynaptic excitatory sites were labeled with anti-homer1 antibody (Fig. 2h). In lamina II of the dorsal horn, VGLUT2 marks terminals of IB4-binding peripheral sensory neurons as well as those of spinal cord excitatory interneurons. To exclude VGLUT2$^+$ terminals of sensory neurons from our analysis, we only quantified pairs between VGLUT2$^+$ terminals and homer1$^+$ postsynaptic puncta that were IB4 negative (Supplementary Figs. 2a1-2 and 2b1-2). Quantifications of VGLUT2$^+$ IB4$^-$ excitatory synapses showed no difference between ipsilateral and contralateral dorsal horns in vehicle-treated animals (vehicle: $t_{96} = 0.3$, $P > 0.99$) (Fig. 2j). Surprisingly, microglial depletion resulted in a 13% increase in ipsilateral dorsal horn excitatory synapse density (PLX3397: $t_{96} = 2.5$, $P = 0.0232$) (Fig. 2j). Taken together, these findings demonstrate that transient microglial depletion during the peak period of synapse pruning reduces mechanical hypersensitivity, prevents both excitatory and inhibitory synapse removal, and ultimately prevents the selective loss of dorsal horn inhibitory synapses in the SNI model of neuropathic pain. Since microglia contribute to pain behavior through multiple pathways, the specific contribution of their synapse removal capacity to pain phenotype cannot be conclusively determined from microglial depletion approaches. To address this, we next identified the microglia-driven synapse removal pathway involved in neuropathic pain and examined the effects of blocking this pathway on pain behavior.

Peripheral nerve injury induces upregulation of the components of spinal complement and CX3CR1-mediated synapse pruning pathways

We next investigated which microglial synapse pruning pathway mediates elimination of presynaptic terminals in neuropathic pain. RNA-seq data of spinal cord at day 7 post-SNI, when microglial engulfment activity peaks, were analyzed using selected Gene Ontology (GO) annotations and revealed that elements of synapse pruning pathways were significantly up-regulated in the spinal cord of SNI mice as compared to naive animals (ES = +0.99, $P = 1.0 \times 10^{-2}$, FDR = 11%)[26]. Specifically, genes related to complement pathway (i.e., *C1qa*, *C1qb*, *C1qc*, *C4, and Itgam*) and fractalkine receptor (CX3CR1) pathway (i.e., *Cx3cr1*), two main molecular pathways associated with synapse pruning, were significantly increased (Fig. 3a). Further analysis of single-cell RNA sequencing dataset[27] revealed upregulation of complement and CX3CR1 mediated synapse pruning transcripts in disease-associated microglia at day 14 post-SNI (Supplementary Fig. 3a: clusters 1-6). Consistent with our previous findings from engulfment analyses, we did not find significant gene expression changes associated with synapse pruning at day 3 post-SNI (Supplementary Fig. 3a). We next assessed protein levels of the main signaling molecules within these pathways in the spinal cord of neuropathic mice.

In the complement-mediated synapse pruning pathway, C1q and C3-derived complement fragment C3b are localized to vulnerable synapses, promoting microglia-mediated synaptic engulfment via microglial C3 receptor (CR3) (Fig. 3b)[13]. Quantifications of C1q, and C3 protein levels in the dorsal horn of neuropathic mice at day 7 after nerve injury revealed a significant increase in C1q and C3 expression (C1q: $t_9 = 17.9$, $P < 0.0001$; C3: $t_9 = 5.6$, $P = 0.0003$) (Figs. 3c1-2, and 3d1-2). Moreover, the number of CR3 immunoreactive microglia was also significantly increased (≈ 3.5-fold) in the ipsilateral dorsal horn at day 7 post-injury (CR3: $t_7 = 11.7$, $P < 0.0001$) (Figs. 3e1-2). Temporal analysis of C1q, C3, and CR3 expression in laminae I-II showed an earlier and greater increase in CR3 levels starting at day 3 following injury (Fig. 3f). This was followed by an increase of C1q and C3 at days 7, 14, and 21 post-SNI (Fig. 3f). At 5 months post-SNI, when chronic neuropathic pain is well-stablished in the absence of injury-associated inflammation, expression levels of C1q and CR3 were significantly reduced compared to day 7 post-SNI but remained elevated compared to contralateral side (C1q (D7 vs. M5): $t_8 = 2.5$, $P = 0.0348$; CR3(D7 vs. M5): $t_8 = 2.6$, $P = 0.0278$) (Fig. 3f, and Supplementary Figs. 3a, 3b1-2, and d1-2). At 5 months post-SNI, ipsilateral C3 levels were significantly reduced compared to day 7 (C3 (D7 vs. M5): $t_8 = 3.3$, $P = 0.01$) (Fig. 3f and Supplementary Figs. 3a and 3c1-2).

The other major synapse pruning pathway identified in our RNA-seq dataset operates through the binding of the neuronal chemokine fractalkine (CX3CL1) to its microglial receptor CX3CR1 (Fig. 3b)[14]. We observed immunoreactivity of CX3CL1 in the dorsal horn of the spinal cord, however, further analysis of CX3CL1 expression showed no injury-dependent overall change (Figs. 3g1-2). Conversely, there was a significant increase in the number of CX3CR1$^+$ microglia at day 7 post-SNI ($t_{10} = 5.9$, $P = 0.0001$) (Figs. 3h1-2), as well as increased CX3CR1 expression per individual microglia cell ($t_{20} = 3.4$, $P = 0.0026$) (Figs. 3i1-2). Temporal analysis of CX3CR1 expression after injury revealed a stable increase, starting at day 3, which persisted for 5 months post-SNI (Fig. 3j). At 5 months post-SNI, we found no significant microglia-mediated engulfment of inhibitory (Supplementary Fig. 3e1-2) and excitatory (Supplementary Fig. 3f1-2) terminals, which was consistent with downregulation of major synapse pruning-associated complement proteins. Notably, at this chronic time-point, a significant decrease in inhibitory synapses ($t_8 = 2.3$, $P = 0.03$) and an increase in excitatory synapses ($t_8 = 3.4$, $P = 0.009$) were observed in the ipsilateral LII as compared to the contralateral side, suggesting a lasting effect of synapse engulfment on dorsal horn connectivity (Supplementary Figs. 3e3-4, and 3f3-4). Taken together, these experiments provide evidence for the upregulation of CX3CR1 and components of complement-mediated synapse pruning pathways in the SNI model of neuropathic pain.

Nerve injury-induced engulfment of spinal presynaptic terminals is mediated by the complement pathway

Nerve injury-induced increases of the components of the complement and CX3CR1 mediated pruning pathways suggest that these pathways might be involved in synapse pruning in the spinal cord. To assess the respective contribution of the complement and CX3CR1 pathways to spinal cord synapse removal in neuropathic pain, levels of engulfment

https://doi.org/10.1038/s41467-025-59849-1

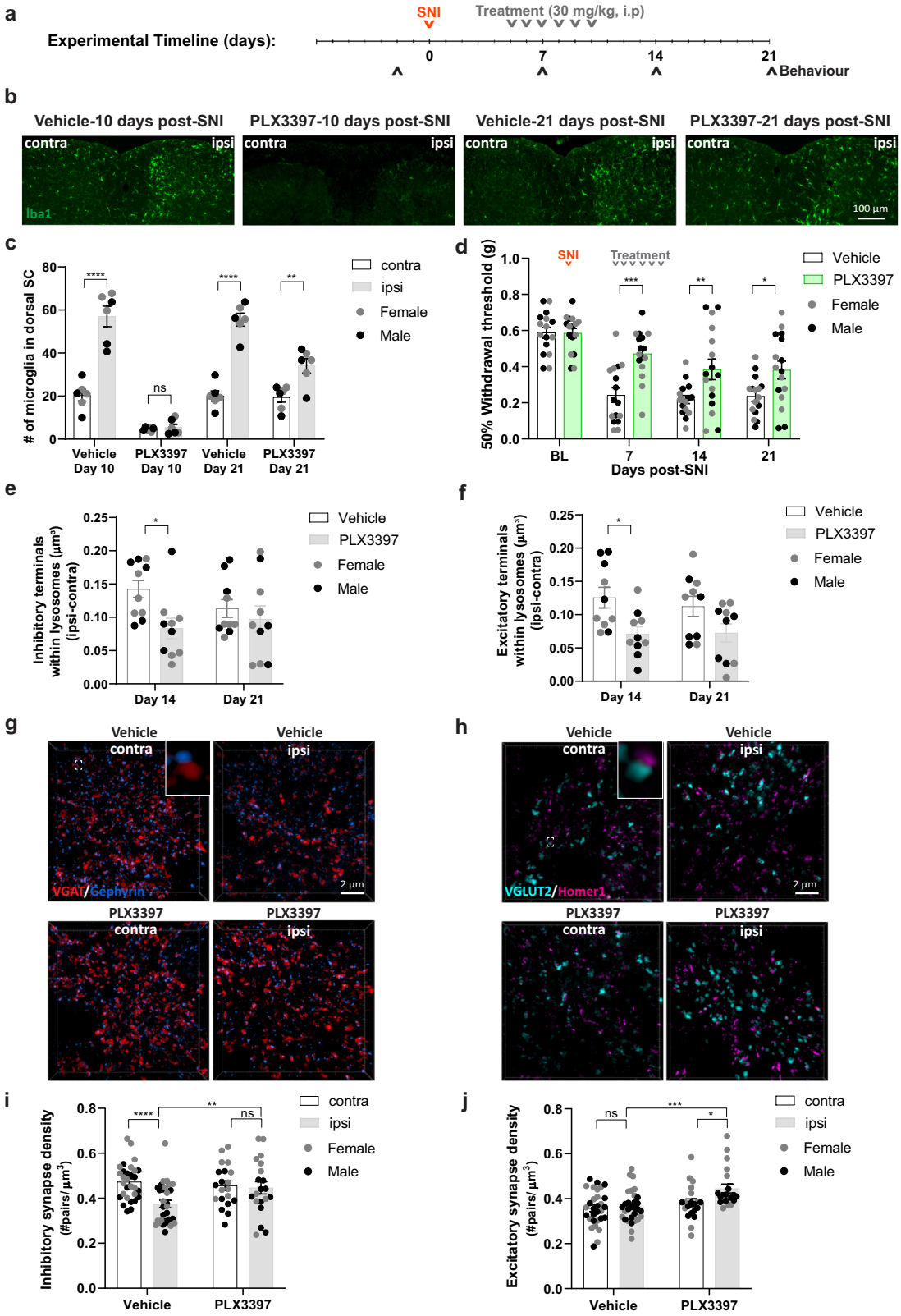

of inhibitory and excitatory presynaptic terminals were measured at the peak of synapse engulfment (i.e., 7 days after SNI) in mice lacking complement factor C3 (C3 KO) or CX3CR1 (CX3CR1 KO). In both KO mouse lines, peripheral nerve injury induced microgliosis (C3 KO: $t_{30} = 8.7$, $P < 0.0001$; CX3CR1 KO: $t_{30} = 6.0$, $P < 0.0001$) (Supplementary Figs. 4b1) and a significant increase in the volume of CD68$^+$ lysosomal compartments in the ipsilateral dorsal horn (C3 KO: $t_{30} = 4.2$, $P = 0.0006$; CX3CR1 KO: $t_{30} = 3.1$, $P = 0.0104$) (Supplementary Figs. 4b2-3). Although the increase in the number of microglia and CD68$^+$ lysosomal volume in CX3CR1 KO mice was smaller as compared to C3 KOs and wildtype (WT) littermates (Supplementary Figs. 4b2-3), comparable levels of engulfed inhibitory and excitatory terminals were still detected within CX3CR1 KO lysosomes in the ipsilateral dorsal horn (Figs. 4a1-2 and 4b1-2).

Fig. 2 | Transient microglia depletion during the peak of synapse engulfment prevents the normal development of mechanical hypersensitivity and protects dorsal horn synaptic connectivity. a Diagram showing the timeline of drug treatment, SNI surgery, and behavioral tests. **b** Dorsal horn images labeled for Iba1 (green) from vehicle and drug (PLX3397) treated groups from the last day of treatment and after a 10-day wash-out period. **c** Quantification of the number of microglia in dorsal spinal cord ($n = 6$ mice per group; 3 mice per sex). **d** Pain behavior in neuropathic mice treated either with PLX3397 or vehicle ($n = 16$ mice per group; 8 mice per sex). **e**, **f** Quantifications of relative engulfment of inhibitory (**e**) and excitatory (**f**) terminals at 14 and 21 days-post SNI when microglia repopulate the spinal cord ($n = 9$ mice per group; 5 male mice and 4 female mice). **g** Representative SIM images of inhibitory synapses labeled with a pre-synaptic marker (VGAT; red) and a post-synaptic marker (gephyrin; blue) in different conditions. The inset within the first image is an enlarged view of an inhibitory synapse. **h** Representative SIM images of excitatory synapses labeled with a pre-synaptic marker (VGLUT2; cyan) and a post-synaptic (homer1; magenta) in different conditions. The inset within the first image is an enlarged view of an excitatory synapse. **i** Quantification of inhibitory synapse density ($n = 30$ mice per vehicle group; $n = 20$ mice per PLX3397 group; 10–15 mice per sex). **j** Quantification of inhibitory synapse density ($n = 30$ mice per vehicle group; $n = 20$ mice per PLX3397 group; 10–15 mice per sex). Means are plotted with individual data points ± SEM. $^{*}p < 0.05$, $^{**}p < 0.01$, $^{***}p < 0.001$ and $^{****}p < 0.0001$ analyzed with repeated measures two-way ANOVA with Bonferroni post hoc test (**d**) and two-way ANOVA with Bonferroni post hoc test (**c**, **e**, **f**, **i**, **j**). Source data are provided as a Source Data file.

Notably, C3 KO mice showed no engulfment of inhibitory and excitatory presynaptic terminals as demonstrated by reductions in the total volume of VGAT and VGLUT2 immunoreactive puncta within microglial lysosomes (Figs. 4a1-2 and 4b1-2). Therefore, these results indicate that the complement pathway, but not the CX3CR1 pathway, is essential for increased engulfment of terminals by microglia in the SNI model of neuropathic pain.

We next evaluated the role of complement and CX3CR1 pruning pathways in remodeling dorsal horn synaptic connectivity in the SNI model of neuropathic pain. To this end, we quantified inhibitory and excitatory synapse densities in C3 KO and CX3CR1 KO mice 21 days after injury. Similar to WT mice, we found a 21% decrease in ipsilateral inhibitory synapse density (i.e., VGAT puncta juxtaposed gephyrin puncta) in CX3CR1 KO mice as compared to the contralateral side (CX3CR1 KO: $t_{42} = 3.3$, $P = 0.0048$) (Figs. 4c1-2). In contrast, the decrease in ipsilateral dorsal horn inhibitory synapses was prevented in C3 KO mice (Figs 4c1-2). Quantification of excitatory synapses showed no change in VGLUT2^{+} excitatory synapse density in CX3CR1 KO mice as compared to WT animals (Figs. 4d1-2). However, ipsilateral dorsal horn VGLUT2^{+} excitatory synapse density in C3 KOs was increased by 9% as compared to the contralateral side ($t_{42} = 4.2$, $P = 0.0104$) (Fig. 4d2). Interestingly, a comparison of contralateral dorsal horn synapse densities revealed that C3 KO mice had a 20% increase in inhibitory synapse density and 24% increase in excitatory synapse density as compared to WT littermate controls, indicating a potential developmental deficit in refinement of dorsal horn synaptic connections in the C3 KO mice (Figs. c2 and d2). To address the involvement of the complement pathway in spinal synaptic development, we examined spinal synapse engulfment in WT, and mice lacking complement factor C4 (C4 KO) and C3 (C3 KO) at postnatal day 7. At this age, we observed microglia-mediated engulfment of inhibitory and excitatory inputs in WT mice (Figs. 4e1-2, and 4f1-2). Conversely, spinal microglia sampled from P7 C4 or C3 KO mice had a significant decrease in capacity to engulf inhibitory and excitatory terminals as compared to WT littermate controls (Figs 4e3 and 4f3). Additionally, we observed that C4 and C3 KO mice had a comparable deficit in synapse pruning at 7 days post-SNI (Figs. 4e4 and 4f4). Taken together, these data implicate the complement synapse pruning pathway, but not the CX3CR1 pathway, as the mechanism that modulates dorsal horn synaptic connectivity both during spinal development and in the presence of neuropathic pain.

Complement protein C1q is expressed by nerve injury-activated microglia and localized to dorsal horn synapses

Complement protein C1q is the initiating factor of the classical complement cascade and has been implicated in the selective elimination or "pruning" of synapses through the complement pathway[13]. C1q levels are tightly regulated in the adult CNS, while injury, normal aging, or certain diseases increase C1q expression[16,28,29]. Previous findings with respect to the CNS have revealed that both neurons and glia are capable of synthesizing C1q[30,31]. To determine whether neurons are the source of C1q in neuropathic pain, we performed fluorescent in situ hybridization for *C1qa* mRNA on spinal cord sections of Gad2-tdTom and Tac1-tdTom mice collected 7 days post-injury (Figs. 5a1-2). Consistent with the RNA-seq data, *C1qa* mRNA was upregulated (≈ 8-fold) as assessed by the number of *C1qa* mRNA immunoreactive puncta per DAPI^{+} dorsal horn cell nuclei ($t_8 = 11.2$, $P < 0.0001$) (Fig. 5a1 and 5a3). Interestingly, the *C1qa* mRNA signal was almost completely excluded from Gad2^{+} and Tac1^{+} cell bodies, suggesting that these cells are not the source of *C1qa* (Figs. 5a2 and 5a4). We next examined the expression pattern of C1q protein in the dorsal horn of neuropathic mice. We observed strong and distinct microglia-specific C1q immunoreactivity, which was significantly elevated in the ipsilateral dorsal horn ($t_{10} = 6.3$, $P < 0.0001$) (Figs. 5b1-2). In addition to the marked increase of C1q protein within microglia, a relatively smaller, punctate signal was scattered outside of microglia and was only found in the ipsilateral dorsal horn (Supplementary Fig. 5a). To test if this extracellular C1q signal was associated with synaptic structures, we performed SIM on spinal cord sections immunolabeled for C1q as well as presynaptic markers for inhibitory (VGAT^{+}) and excitatory (VGLUT2^{+}) synapses. Consistent with our prediction, most extracellular C1q signals were in close proximity to presynaptic markers (Figs. 5c1-2). Quantification of the number of synapses in close proximity to C1q revealed a higher percentage of both inhibitory and excitatory synapses tagged with C1q in the ipsilateral dorsal horn as compared to the contralateral side (VGAT: $t_{36} = 12.4$, $P < 0.0001$; VGLUT2: $t_{36} = 3.5$, $P = 0.0024$) (Fig. 5c3). Interestingly, a larger proportion of inhibitory synapses was marked by C1q than excitatory synapses ($t_{18} = 9.1$, $P < 0.0001$) (Fig. 5c3). To determine whether the C1q deposited on synapses is secreted by microglia, we chronically depleted microglia using PLX3397 and assessed C1q protein expression in the dorsal horn at day 7 post-injury. Depletion of microglia resulted in almost complete elimination of C1q immunoreactivity in the dorsal horn, including C1q depositions on synapses (Figs. 5d1-4).

After establishing that C1q is released from nerve injury-activated microglia and deposited on synapses, we investigated whether expression of the apoptotic protein, cleaved caspase-3 (CC3), contributed to the recruitment of C1q to vulnerable synapses[32]. To answer this question, we analyzed inhibitory and excitatory presynaptic terminals for the presence of CC3 and C1q. Co-localization analysis showed that CC3 signal was rarely found at presynaptic terminals, and this was independent of C1q deposition at the synaptic site (Supplementary Figs. 5b1-3). This indicates that CC3 does not drive injury-induced synapse pruning in the spinal cord. Together, these results demonstrate that C1q protein is produced by microglia and preferentially, but not exclusively, marks dorsal horn inhibitory synapses for elimination in the SNI model of neuropathic pain.

Inhibiting C1q interferes with the establishment of neuropathic pain and protects dorsal horn synaptic circuitry

To determine whether induction of C1q expression in response to peripheral nerve injury causes synaptic reorganization in the spinal dorsal horn, we pharmacologically blocked C1q using anti-C1q antibodies (ANX M1.21). Anti-C1q antibodies were administered

https://doi.org/10.1038/s41467-025-59849-1

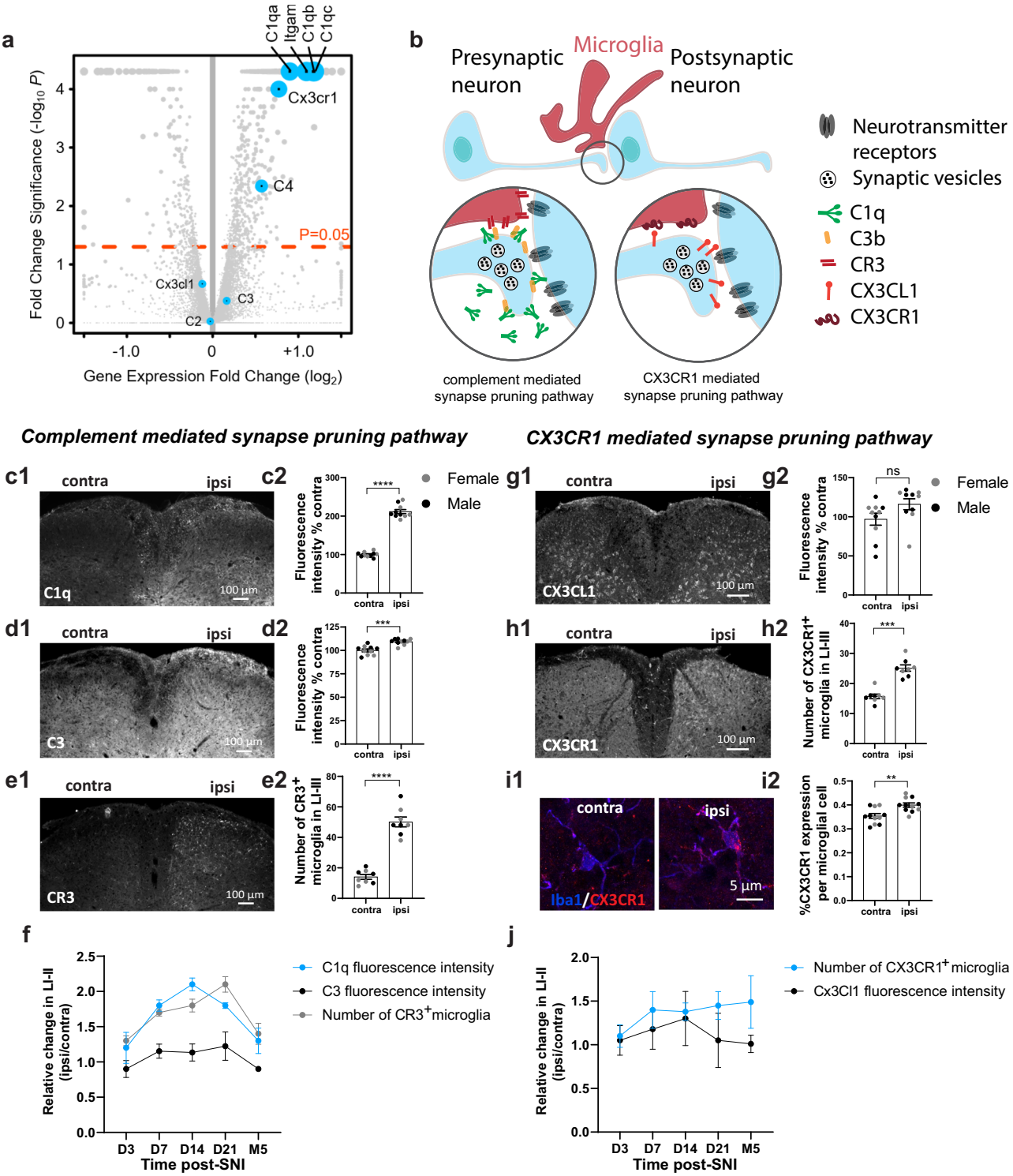

intraperitoneally every 4 days, starting 24 hours before SNI surgery. This treatment regimen resulted in full inhibition of the classical complement pathway (Supplementary Fig. 6a) and was sufficient to inhibit C1q expression in the target tissue, as demonstrated by positive anti-drug staining in the spinal cord of mice treated with ANX M1.21 (Supplementary Figs. 6b1-6). To assess pain behaviour, mechanical hypersensitivity associated with neuropathic pain was measured weekly (Fig. 6a). Mice in both control (IgG isotope) and drug-treated groups developed mechanical hypersensitivity as shown by decreases in withdrawal thresholds of the ipsilateral hind paw (Fig. 6b). Notably, at day 21 after injury, unlike IgG-isotope control-treated mice, both male and female ANX M1.21-treated animals showed a significant reduction in mechanical hypersensitivity ($t_{152} = 13.2$, $P = 0.0065$) (Fig. 6b). Furthermore, we found that ANX M1.21 resulted in a significant decrease in total C1q (Supplementary Fig. 6b7) and extracellular C1q (Supplementary Fig. 6c1-3) ($t_{36} = 4.6$, $P < 0.0001$). Additionally, SIM revealed a marked decrease in the number of ipsilateral C1q-associated inhibitory and excitatory synapses in ANX M1.21-treated groups as compared to IgG-isotope control-treated mice (VAGT: $t_{10} = 5.6$, $P = 0.0002$; VGLUT2: $t_{10} = 3.2$, $P = 0.0085$) (Figs. 6c1-2).

To study whether the effect of ANX M1.21 on neuropathic pain behavior was associated with disruption of the complement and

Fig. 3 | Complement and CX3CR1 mediated synapse pruning proteins are upregulated in neuropathic pain. a Volcano plot showing gene expression changes in neuropathic mice at day 7 post SNI. Each dot is a gene. Positive fold change indicates higher expression in the spinal cord of SNI-injured mice than in naïve. Genes highlighted in blue are related to complement and CX3CR1 pruning pathways. Dashed horizontal orange line indicates *P*-value of 0.05. **b** Drawing illustrates microglia and signaling molecules that participate in complement and CX3CR1 pruning mechanisms. **c1-e1** Representative images of C1q, C3, and CR3 labeling in the dorsal horn of SNI mice at day 7 post-SNI. **c2-e2** Quantifications of fluorescence intensity of dorsal horn C1q, and C3, as well as number of $CR3^+$ microglia in laminae I-III ($n = 8$ mice per group; 4 mice per sex). **f** Temporal expression changes of ipsilateral C1q, C3, and CR3 levels normalized to the contralateral side ($n = 5$ mice per group; 3 males and 2 females). **g1-h1** Representative dorsal horn images of CX3CL1 and CX3CR1 immunolabelling in SNI mice at day 7 post-SNI. **g2-h2** Quantifications of fluorescence intensity of dorsal horn CX3CL1, and the number of $CX3CR1^+$ microglia in laminae I-III ($n = 8$ mice per group; 4 mice per sex). **i1** High-resolution image of CX3CR1 (red) expression in microglia (blue) sampled from ipsilateral and contralateral dorsal horn (quantified **i2**) ($n = 8$ mice per group; 4 mice per sex). **j** Temporal expression changes of ipsilateral number of CX3CR1+ microglia and CX3CL1 fluorescence intensity levels normalized to the contralateral side ($n = 5$ mice per group; 3 males and 2 females). For transcriptomics, false discovery rate (FDR) is used to correct for multiple two-sided t-tests (**a**). Means are plotted with individual data points ± SEM. $^{**}p < 0.01$, $^{***}p < 0.001$, and $^{****}p < 0.0001$ analyzed with paired two-tailed t-test (**c2-h2**) and unpaired two-tailed t-test (**i2**). ns, analyzed with two-tailed t-test comparing day 3 and month 5 time points (**f**, **j**). Source data are provided as a Source Data file.

microglia-mediated synapse pruning pathway, we quantified engulfment of inhibitory and excitatory terminals by microglia in control and drug-treated animals. In line with our prediction, there was a significant reduction in inhibitory and excitatory presynaptic elements within ipsilateral microglial lysosomes of ANX M1.21-treated mice compared to controls (inhibitory synapse engulfment: $t_{36} = 12.7$, $P < 0.0001$; excitatory synapse engulfment: $t_{36} = 2.8$, $P = 0.0136$) (Figs. 6d1-2 and 6e1-2). To test whether blocking C1q protects against nerve injury-induced synapse loss, we conducted synapse quantification in the dorsal horn of ANX M1.21 and IgG control mice 21 days after injury. ANX M1.21 prevented inhibitory synapse loss and resulted in an increase of excitatory synapses in the spinal dorsal horn (Figs 6f1-2 and 6g1-2). This effect on spinal synapse density was similar to our previous observations with PLX3397 treatment and in C3, and C4 KO mice (ipsilateral inhibitory synapses: $t_{76} = 5.8$, $P < 0.0001$; ipsilateral excitatory synapses: $t_{76} = 5.2$, $P < 0.0001$). Altogether, these results demonstrate that targeting C1q, the initiating signaling protein of the complement-mediated synapse pruning pathway, protects the dorsal horn synaptic network and attenuates chronic neuropathic pain by inhibiting microglia-mediated synapse engulfment.

Discussion

We have identified a mechanism by which microglia contribute to neuropathic pain through reorganization of the synaptic network in the spinal dorsal horn. We show that following peripheral nerve injury, activated microglia engage the classical complement pathway to remove spinal synapses. This is accomplished via the production and release of complement protein C1q, which is deposited on spinal synapses to tag them for removal through complement-dependent microglial signaling. Pharmacological inhibition of C1q protected spinal cord circuitry and prevented inhibitory synapse loss by disrupting synapse engulfment, thereby ameliorating neuropathic pain. These data implicate complement-mediated synapse pruning as a major driver of structural synaptic plasticity in neuropathic pain and identify a therapeutic strategy to prevent the maintenance of the pain hypersensitivity.

Activation of spinal complement-mediated synapse pruning in neuropathic pain

It is well established that microglia-mediated synapse pruning plays a key role in sculpting a functional neural network within the developing central nervous system[12]. Emerging research has implicated various microglial signaling pathways in this process, many of which are reactivated later in life in different neurological disorders[16,17,33]. For example, pathological involvement of complement mediated synaptic pruning has been implicated in Alzheimer's disease, frontotemporal dementia, and schizophrenia[16,17,34]. Meanwhile, CX3CR1 signaling is implicated in epilepsy and sensory lesion-induced synaptic pruning[15,35]. Given the induction of both the complement and CX3CR1 pathways in the spinal cord after nerve injury, we explored the possibility of their involvement in the remodeling of dorsal horn circuits in neuropathic pain. The evidence for a role of the complement-mediated synapse pruning in neuropathic pain was abundant, as specific disruptions at multiple levels of the pathway protected both dorsal horn inhibitory and excitatory synapses and prevented synapse engulfment. Unlike the complement pathway, the CX3CR1 pathway did not appear to play a significant role in dorsal horn synapse pruning. The modest reduction in engulfment of excitatory synapses in neuropathic CX3CR1 KO mice can be explained by other defects in CX3CR1-deficient microglia, including interference with cell functions, such as cell adhesion and motility, which affect microglial phagocytic activity necessary for synapse pruning[36,37].

Apart from synapse pruning, phagocytosis-related receptors, such as P2Y12, P2Y6, and TMEM16F, are upregulated in neuropathic pain models and pharmacological blockade or genetic deletion of these receptors reduce neuropathic pain[38–40]. Many of these receptors have been implicated in synapse removal in other contexts[41,42]. While we cannot rule out the possibility that these pathways might also contribute to dorsal horn synapse removal in neuropathic pain, our data indicate that the complement pathway has a central role in this process. The complete protection of the dorsal horn synaptic network in C3 and C4 KOs as well as in mice treated with a C1q inhibitor supports the notion that the complement pathway is necessary for spinal synaptic remodelling in neuropathic pain.

Microglia rewire dorsal horn circuitry in neuropathic pain

Our data demonstrate that microglia reorganize dorsal horn synaptic circuitry in neuropathic conditions through complement-dependent signaling. This function of microglia results in two key changes in the dorsal horn synaptic network: 1) a major deficit in inhibitory synapses; 2) reorganization of excitatory synapses without an apparent decrease in excitatory synapse density. In contrast to what was observed in inhibitory synapses, the elevated engulfment of excitatory synaptic terminals did not lead to a net loss of excitatory synapses. Notably, at the peak of synapse engulfment activity, excitatory synapse uptake was smaller than the engulfment of inhibitory synapses. This suggests that a compensatory mechanism, specific to the excitatory system, is in place to replenish excitatory synapses. Interestingly, blocking overall microglial synapse engulfment results in an increase in excitatory synapse density, unmasking the dynamic process of excitatory synapse formation in the spinal cord. This is consistent with emerging studies demonstrating activity-dependent excitatory synaptogenesis as a contributing mechanism to neuropathic pain[43,44]. Interestingly, the dynamics of dorsal horn excitatory synapses in neuropathic pain resembles the later phase of development when excitatory synaptogenesis accompanies synapse pruning[45]. Much like development, in neuropathic pain, spinal inhibition is highly compromised, and the spinal cord microenvironment is fueled with neurotrophic and neuromodulating factors to support excitatory synaptic plasticity[6,46,47].

One of the fundamental pathological features of neuropathic pain is the imbalance between excitation and inhibition of dorsal horn

https://doi.org/10.1038/s41467-025-59849-1

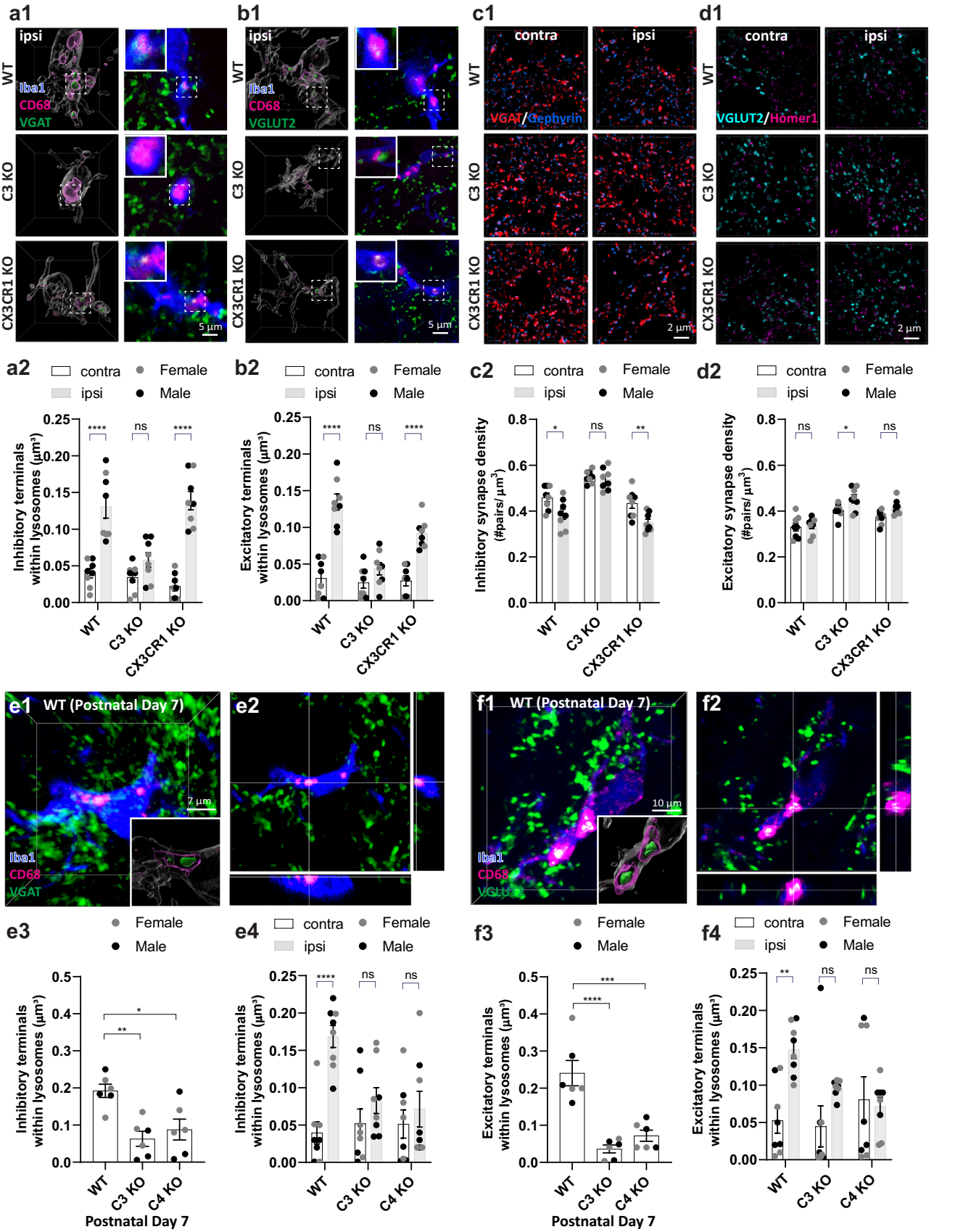

neuronal circuits[48,49]. In this study, we provided a neuroanatomical basis for this imbalance, which is mediated by synaptic pruning activity of reactive microglia. At the molecular level, our results show that C1q deposition on synapses is necessary for the recruitment of microglia to the synapse. Interestingly, we found that within the spinal cord of neuropathic mice, C1q has a greater preference for inhibitory synapses compared to excitatory synapses, which can explain the differential levels of engulfment between inhibitory and excitatory synapses at the

Fig. 4 | Nerve injury-induced engulfment of presynaptic terminals is mediated by the complement pathway. a1 and **b1** First column images represent surface rendering 3D microglia reconstructions (white) sampled from ipsilateral dorsal horns of neuropathic wildtype (WT), C3 KOs, and CX3CR1 KOs demonstrating lysosome (magenta) co-localization with VGAT$^+$ inhibitory (**a1**) and VGLUT2$^+$ excitatory (**b1**) pre-synaptic markers (green). Second column shows single plane images from confocal stacks illustrating the presence or absence of CD68$^+$ lysosomal co-localization with synapse markers. **a2** and **b2** Quantifications of engulfment of inhibitory (**a2**) and excitatory (**b2**) presynaptic terminals by microglia in different genotypes (i/ = 8 mice per group; 4 mice per sex). **c1** and **d1** Three-dimensional representative SIM images of inhibitory (**c1**: VGAT in red and gephyrin in blue) and excitatory (**d1**: VGLUT2 in cyan and homer1 in magenta) terminals captured from dorsal horns of WT, C3 KO, and CX3CR1 KO neuropathic mice. **c2** and **d2** Quantifications of dorsal horn inhibitory (**c2**) and excitatory (**d2**) synapse densities for neuropathic mice of different genotypes ($n = 8$ mice per group; 4 mice per sex). **e1** and **f1** 3D fluorescent images of P7 microglia (blue) sampled from ipsilateral dorsal horn labeled for lysosomal marker CD68 (magenta), marker of presynaptic inhibitory terminals (VGAT; green) (**c1**) and marker of presynaptic excitatory terminals (VGLUT2; green) (**f1**). **e2** and **f2** are single plane enlarged images from confocal stacks illustrating the presence of synaptic signal inside lysosomes. Insets within raw images are surface rendered microglia illustrating engulfment of presynaptic terminals. **e3** and **f3** Quantifications of engulfment of inhibitory (**c3**) and excitatory (**f3**) presynaptic terminals by P7 microglia in WT, C4, C3 KOs ($n = 5$ mice per group; 3 mice per sex). **e4** and **f4** Quantifications of engulfment of inhibitory (**e4**) and excitatory (**f4**) presynaptic terminals by microglia in different genotypes ($n = 8$ mice per group; 4 mice per sex). Means plotted with individual data points ± SEM. $^*p < 0.05$, $^{**}p < 0.01$, $^{***}P < 0.001$, and $^{****}P < 0.0001$ analyzed with two-way ANOVA followed by Bonferroni post hoc test. Source data are provided as a Source Data file.

peak of synapse pruning in this model. It is possible that distinct changes in neuronal activity between inhibitory and excitatory dorsal horn neurons trigger cell type-specific expression of C1q receptors or other recognition molecules at the synapse site[32,50]. This preferential removal of inhibitory synapses, in addition to the failure of the inhibitory system to compensate for the net synapse loss, could contribute to the imbalance between inhibition and excitation, leading to increased excitability in neuropathic pain. This is particularly important for the generation of central sensitization, an enhancement in the activity of nociceptive pathways in response to sensory stimuli[51]. Future studies are necessary to uncover the connection between neuronal activity and production of signaling molecules that attract C1q to the synapse site in neuropathic pain.

Targeting C1q interferes with the maintenance of neuropathic pain

Importantly, we showed that chronic inhibition of C1q is only effective at reducing neuropathic pain at 21 days post-SNI, but not at earlier time points assessed. The delayed effect of anti-C1q antibody treatment suggests that the structural remodeling of the dorsal horn synaptic circuitry is important for the maintenance but not initiation of neuropathic pain. Moreover, despite the robust effects of inhibiting C1q in reducing mechanical hypersensitivity in neuropathic mice, it is important to note that inhibition of C1q does not fully eliminate neuropathic pain behavior. The overall increase of excitatory synapses in the anti-C1q-treated group may contribute to the incomplete reversal of pain behavior. To explore this possibility, both synaptogenesis and synapse pruning should be inhibited concurrently. This would require genetic tools to allow for the selective and simultaneous manipulation of both pathways.

In this study, prophylactic anti-C1q treatment was utilized to investigate the underlying mechanisms of spinal synapse pruning in neuropathic pain. The observed analgesic effects of this treatment suggest that C1q inhibition holds promising therapeutic potential for neuropathic pain management. Although we did not directly assess the post-injury effects of complement inhibition, the temporal characterization of synapse pruning (Fig. 1) and complement expression levels (Fig. 3) suggest that anti-C1q treatment may achieve the greatest analgesic benefit if administered around the second week following peripheral nerve injury, coinciding with the peak of synapse pruning and complement expression in this model.

There is growing evidence to support the existence of sexual dimorphism in key microglial pathways implicated in neuropathic pain[52–54]. However, we did not find any obvious sex differences in the complement-mediated pathway as inhibiting C1q was effective at reducing pain in both male and female mice. This suggests that the sexually dimorphic role of spinal microglia in pain is likely due to the contribution of distinct microglial signaling pathways to sensory symptoms at specific time points during the progression of the disease. Similar to the synapse pruning pathway, several other microglia-driven pathological mechanisms may not exhibit clear sexual dimorphism[55–57]. Collectively, these observations underscore the importance of studying both males and females in pain research.

In summary, our results highlight the importance of microglia and complement-mediated synapse pruning in a pathological loss of inhibitory synapses, as well as provide a mechanistic insight for the imbalance between excitation and inhibition in neuropathic pain. Targeting components of this pathway, such as the complement proteins, protected dorsal horn circuitry and prevented the maintenance of neuropathic pain.

Methods

Animals

All mouse experiments were approved by the Animal Care Committee at McGill University and complied with the Canadian Council on Animal Care guidelines. Following weaning, all mice were housed with their same-sex littermates and were kept in a temperature- and humidity-controlled room with a 12-h light/dark cycle and received food and water *ad libitum*. WT C57BL/6 mice (6-8 weeks of age) of both sexes were purchased from The Jackson Laboratory (Bar Harbor, ME) for pharmacology experiments and used to breed mice of both sexes in-house for all remaining experiments. Mice expressing TdTomato under the inhibitory neuron-specific Gad2 promoter (Gad2-tdTom) were generated by crossing Rosa26LSL-tdTomato reporter mouse line (Ai14) (JAX, stock #007908) with Gad2-IRES-Cre mice (JAX, stock #019022). Mice expressing TdTomato under the Tac1 promoter (Tac1-tdTom) were generated by crossing Rosa26LSL-tdTomato reporter mouse line (Ai14) (JAX, stock #007908) with Tac1-IRES2-Cre-D mice (JAX, stock #021877). Mice expressing TdTomato under the Lmx1b promoter (Lmx1b-tdTomato), MrgD promoter (MrgD-tdTomato), and TMEM119 (TMEM119-tdTomato) were generated by crossing Rosa26LSL-tdTomato reporter mouse line (Ai14) (JAX, stock #007908) with Lmx1btm2(cre/ERT2)Rjo/J (JAX: Stock #:031289), Mrgprdtm1.1(cre/ERT2)Wql/J (JAX, stock #031286), and C57BL/6-Tmem119em1(cre/ERT2)Gfng/J (JAX, stock # 031820), respectively. Knock-out (KO) mouse lines include homozygous C3 KO (JAX, stock #003641), C4 KO (provided by Dr. Michael Carroll) and Cx3cr1^{GFP} KO (JAX, stock #005582), which were bred in-house.

Pain behavior

Baseline hind paw withdrawal thresholds and the temporal development of mechanical hypersensitivity in mice were assessed using von Frey filaments and the up-down method of Dixon[58]. Mice were placed inside Plexiglas cubicles (5.3 × 8.5 × 3.6 cm) with a perforated metal floor and were permitted to habituate for at least 1 h prior to testing. Mice were tested using an ascending series of von Frey filaments, starting with the lowest filament (0.008 g) until threshold was reached. In this approach, filaments were applied to the plantar surface of the hind paw for 3 s and responses were recorded. At least 2 consecutive measures were taken on each hind paw and averaged. The 50%

https://doi.org/10.1038/s41467-025-59849-1

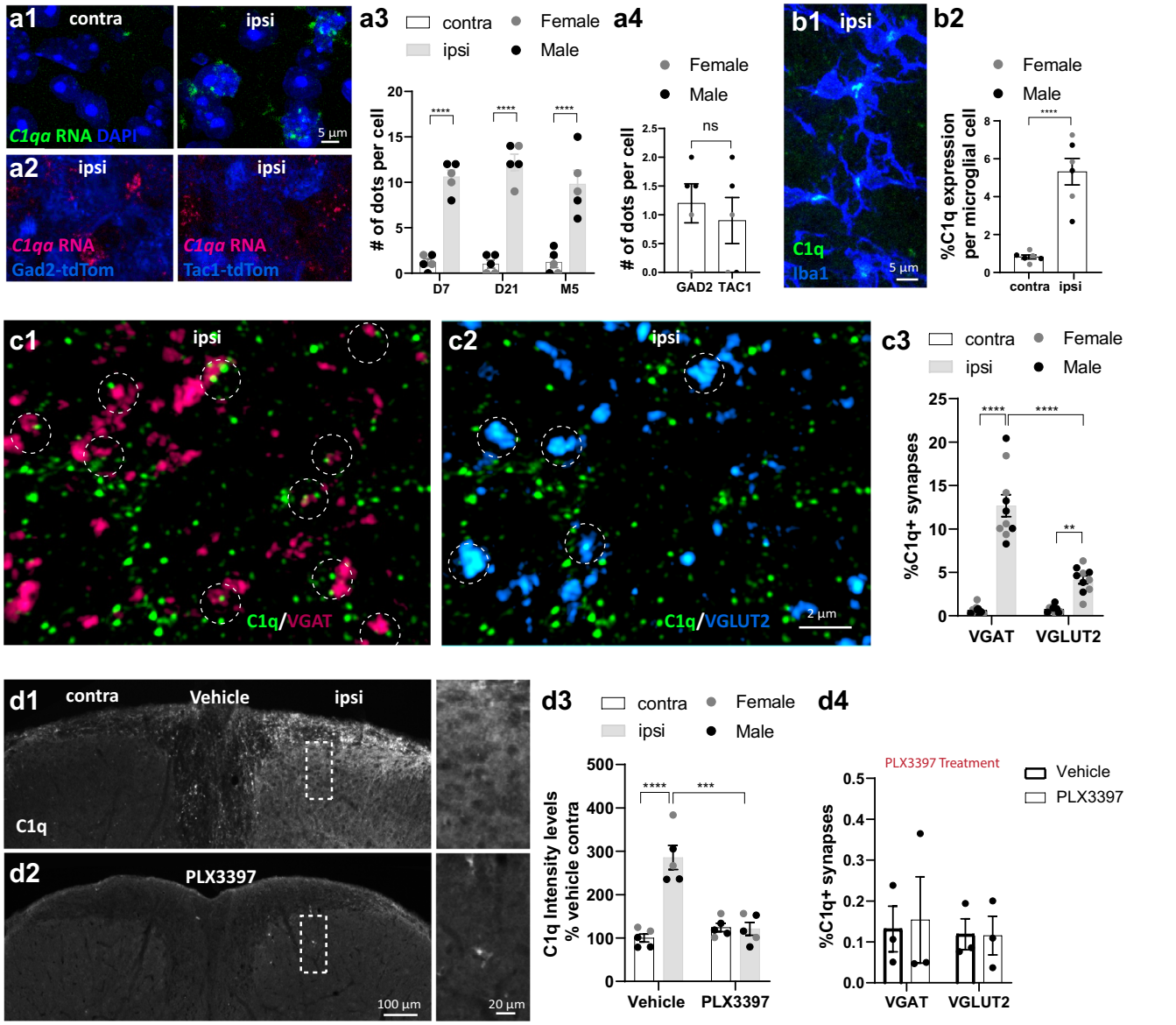

Fig. 5 | Complement protein C1q is expressed by nerve injury-activated microglia and localized to dorsal horn synapses. a1 RNA scope for *C1qa* (**a1**: green) in contralateral and ipsilateral dorsal horn cells (quantified in **a3**) ($n = 5$ mice per group; 3 males and 2 females). Absence of *C1qa* (**a2**: red) expression in inhibitory and excitatory neurons (blue) (quantified in **a4**) ($n = 5$ mice per group; 4 males and 2 females). **b1** Representative high-magnification confocal image of C1q protein (green) in microglia (blue) (quantified in **b2**) ($n = 6$ mice per group; 3 mice per sex). Representative SIM images (**c1-2**) captured from ipsilateral dorsal horn at 7 days post-SNI showing the co-localization of C1q (green) with inhibitory (VGAT in red), and excitatory synapses (VGLUT2 in blue). Dotted circles show synapses that are colocalized with C1q. **c3** Quantifications of C1q co-localization with inhibitory and excitatory synapses ($n = 10$ mice per group; 5 mice per sex). **d1-2** Depletion of C1q expression in the dorsal horn of neuropathic mice chronically treated with vehicle and PLX3397 (quantified in **d3**) ($n = 6$ mice per group; 3 mice per sex). **d4** Quantifications of C1q co-localization with inhibitory and excitatory synapses in vehicle and PLX3397 treated mice ($n = 3$ male mice per group). Means are plotted with individual data points ± SEM. $^{***}p < 0.001$, and $^{****}p < 0.0001$ analyzed by two-way ANOVA with Bonferroni post hoc test (**a3, c3**, and **d3-4**) and unpaired two-tailed t-test (**a4** and **b2**). Source data are provided as a Source Data file.

response threshold was then calculated using the formula: 50% threshold (g) = $10^{(X+kd)}/10^4$, where X = the value (in log units) of the final von Frey filament, k = tabular value for the response pattern and d = the average increment (in log units) between von Frey filaments. All experiments took place during the light cycle and male and female animals were tested on separate days. All experimenters were blinded to the genotype of the mouse and/or the treatment group.

Peripheral nerve injury

In all experiments, mice received a spared nerve injury (SNI) on the left/ipsilateral side, which was performed under isoflurane/oxygen anesthesia as previously described[59]. For this, the sciatic nerve was exposed after making an incision on the skin on the lateral surface of the mouse thigh and sectioning through the biceps femoris muscle. Two of the three terminal branches of the sciatic nerve were tightly ligated with 7.0 silk (Covidien, S-1768K) and 2–4 mm of the nerve distal to the ligation were removed, avoiding any disturbance of the spared nerve. The muscle and skin were closed in separate layers using coated Vicryl (Ethicon, J489G). For experiments in which the sural nerve was left intact (Figs. 1 and 3–6), von Frey testing was performed on the lateral part of the hind paw. In one experiment in which the tibial nerve was intact (Fig. 2), von Frey filaments were targeted to the mid-plantar hind paw[60]. In all experiments, mice were retested for mechanical hypersensitivity every 7 days for 3 weeks.

https://doi.org/10.1038/s41467-025-59849-1

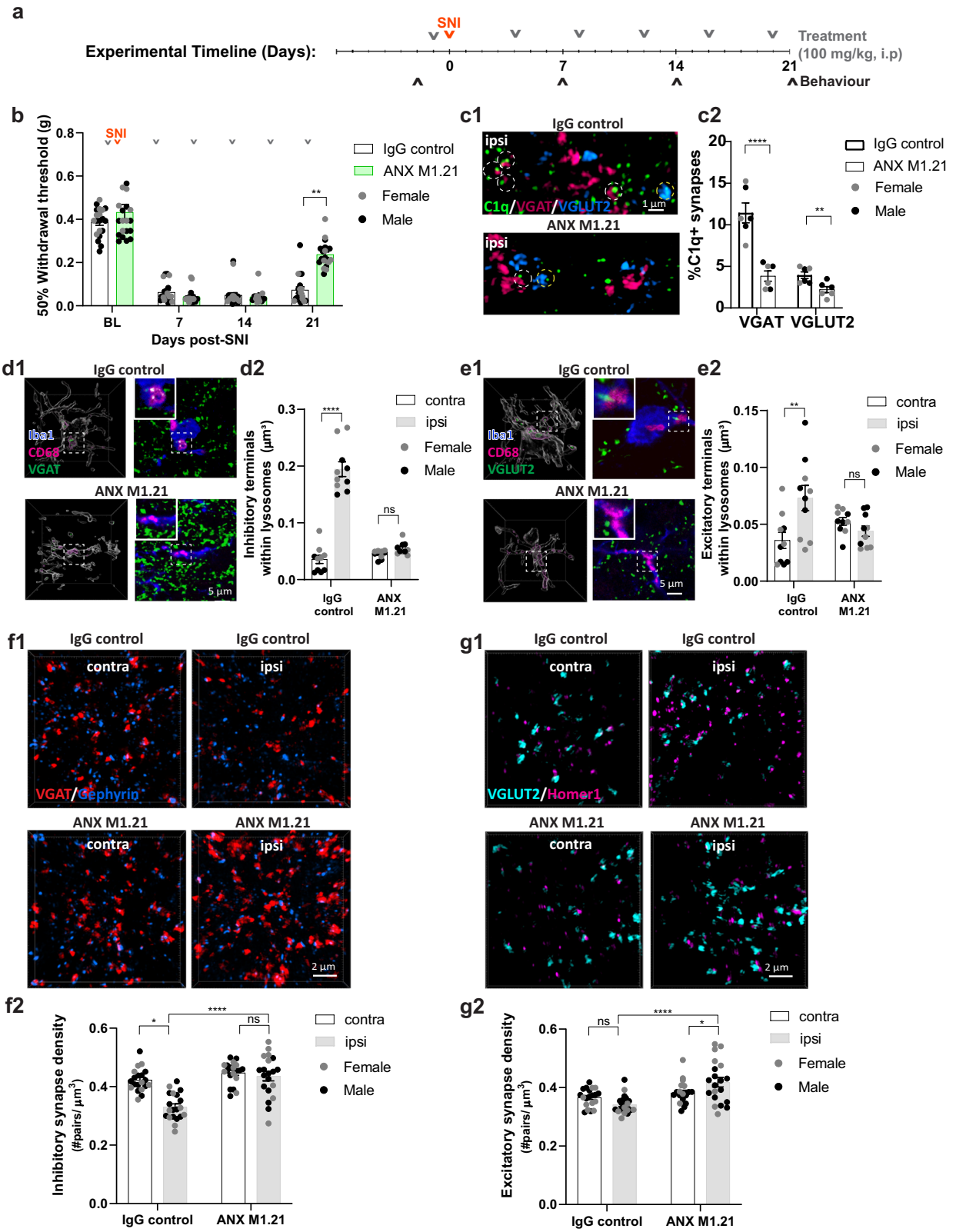

Drugs

PLX3397 (Selleckchem) (30 mg/kg, intraperitoneally (i.p), daily) was dissolved in 10% DMSO + 45% PEG 300 + 5% tween 80 + ddH_2O at 20 mg/ml and administrated for 6 consecutive days. For the C1q neutralizing antibodies experiment, animals received i.p injections of either the ANX-M1.21 anti-C1q function blocking antibody (provided by Annexon Biosciences) or IgG isotype control (provided by Annexon Biosciences) at 100 mg/kg every 4 days starting 1 day prior to peripheral nerve injury until the experimental endpoint.

Tissue preparation and immunohistochemistry

At different time points post-surgery, for immunohistochemistry analyses, mice were anaesthetised (0.3 ml/100 g of body weight of Equithesin containing 6.5 mg of chloral hydrate and 3 mg sodium

Fig. 6 | Functional blocking of C1q interferes with the establishment of mechanical allodynia, protects dorsal horn synaptic circuitry, reduces synapse pruning, and prevents dorsal hornsynapse loss. a A diagram showing the timeline of drug treatments, surgery, and behavior testing. **b** Pain behaviour in neuropathic mice treated either with ANX-M1.21 or IgG control (n = 20 mice per group; 12 males and 8 females). **c1** Representative images from ipsilateral dorsal horn show the co-localization of C1q (green) with inhibitory synapses (VGAT; red), and excitatory (VGLUT2; blue) in different experimental groups (Quantified in **c2**) ($n = 6$ mice per group; 3 mice per sex). **d1** and **e1** Representative 3D surface rendering of microglia (white) from ipsilateral dorsal horn of IgG control and ANX-M1.21 treated mice. A single plane enlarged image selected from the confocal stack illustrating the CD68 (magenta) co-localization with VGAT or VGLUT2 (**d1**, **e1**: green). Insets within 3D reconstructions are enlarged views of VGAT (**d1**) or VGLUT2 (**e1**) co-localization with CD68 (quantified in **d2** and **e2**) ($n = 10$ mice per group; 5 mice per sex). **f1** Representative images of inhibitory presynaptic (VGAT; red) and postsynaptic (gephyrin; blue) elements from different conditions and quantification in **f2** (n = 20 mice per group; 12 males and 8 females). **g1** Representative images of excitatory pre-synaptic (VGLUT2; cyan) and post-synaptic (homer1; magenta) elements from different conditions and quantification in **g2** ($n = 20$ mice per group; 12 males and 8 females). Means are plotted with individual data points ± SEM. $^{*}p < 0.05$, $^{**}p < 0.01$, and $^{****}p < 0.0001$ analyzed with repeated measures two-way ANOVA with Bonferroni post hoc test (**b**) two-way ANOVA with Bonferroni post hoc test (**d2, e2, f2**, and **g2**), and t-test (**c2**). Source data are provided as a Source Data file.

pentobarbital), and perfused transcardially with perfusion buffer (0.5 g/L $NaHCO_3$ in PBS) followed by 4% paraformaldehyde (PFA) in 0.1 M phosphate buffer (PB), pH 7.4, for 10 min. After fixation, spinal cords were extracted and post-fixed in the same fixative overnight at 4 °C and then transferred to 30% sucrose in PB for cryoprotection. For immunohistochemistry, transverse spinal cord sections from the lumbar enlargement (L3–L5) were cut on a cryostat (Leica, Germany) at −20 °C. Twenty-µm-thick sections were prepared for Airyscan confocal microscopy (Carl Zeiss LSM 880) and 10 µm-thick sections were prepared for structural illumination microscopy (SIM) (DeltaVision OMX SR). Sections were then permeabilized and blocked at room temperature for 1 h in 10% normal donkey or goat serum and 0.2% Triton-X in PBS (PBST). This step was followed by incubation of sections in a cocktail of primary antibodies in 5% blocking solution at 4 °C. Primary antibodies were rabbit anti-Iba1 (Wako 019-19741, 1:1000), guinea pig anti-Iba1 (Synaptic Systems 234 004, 1:500), rat anti-CD68 (Bio-Rad NBP2-33337, 1:500), mouse anti-vesicular GABA transporter (VGAT, Synaptic Systems 131 011BT, 1:1000), rabbit anti-VGAT (Synaptic Systems 131 008, 1:2000), rat anti-CD11b (Bio-Rad MCA711, 1:100), guinea pig anti-VGLUT2 (Millipore AB2251-I, 1:2000), mouse anti-gephyrin (Synaptic Systems 147 011, 1:400), rabbit anti-Homer1 (Synaptic Systems 160 003, 1:200), goat anti-mouse C3 (MP Biomedicals 55444, 1:100), rabbit-anti NeuN (Millipore 32160702, 1:1000), rabbit anti-C1q (Abcam 182451, 1:400), goat anti-CX3CL1 (R&D systems AF 537, 1:500), rabbit anti-CX3CR1 (Thermofisher TP501, 1:200), rabbit anti-ANX-M1.21 antibody (provided by Annexon Biosciences, 1:500), mouse monoclonal anti-C3R (Hycult Biotech, 1:500), and mouse monoclonal anti-C5R (Hycult Biotech, 1:500). Twenty-four hours later, appropriate Alexa-fluorophore-conjugated secondary antibodies were applied to sections (Invitrogen, 1:800), which were incubated at room temperature for 2 h. In some experiments, isolectin B4 (IB4) conjugated to Alexa 647 was used in the mixture of secondary antibodies (Invitrogen, 1:200). Sections were then mounted and coverslipped using Prolong Gold Antifade mounting medium (Invitrogen) and Zeiss cover slips. Analyses were carried out in the deeper 2/3 of lamina II (inner lamina II).

Microglia density quantification

Low magnification images were captured using a Zeiss AxioImager M2 Imaging microscope with the Zeiss ZenPro software v.2.3 (Zeiss Canada). For quantification of microglia density, 4 sections per animal were assessed. To capture the entire dorsal horn, a 10X field was imaged. To calculate the density of microglia, the number of microglia was divided by the area of the dorsal horn measured using ImageJ software (NIH).

Engulfment quantification

For assessing phagocytosis of synaptic elements, we used an engulfment quantification method inspired by Schafer and colleagues[61]. Briefly, sections immunolabeled with CD68, Iba1, and a marker for the neuronal structure of interest were imaged by 63x oil immersion objective (NA 1.4) at 0.2 µm z-steps using a Zeiss LSM 880 Airyscan confocal microscope. Images were processed with IMARIS software (Bitplane) to produce 3D surface renderings of the engulfed material within microglial lysosomes, microglia, and lysosomes. Volumes associated with each surface rendered structure were recorded and engulfment measurements for each microglial cell were calculated using the formula: the volume of the engulfed material within lysosomal compartments/the volume of microglial cell. For each animal, graphed values represent the mean of a total of 8 - 12 microglia sampled from 4 sections analyzed. Only microglia that had their full cell bodies imaged were selected for quantification. Imaging parameters, selection criteria, and thresholding values were consistently applied to all quantifications. All experimenters were blinded to the genotype of the mouse, sex, and/or the treatment condition. Blinding to laterality in untreated mice was not possible because of the evident morphological changes in ipsilateral microglia.

Analysis of synaptic elements

SIM was used to assess synapse densities. Cells were imaged with a 100x, NA = 1.42, oil immersion objective on a Vision OMX V_4 Blaze system (GE) equipped with 488 nm, 592 nm, and 647 nm lasers and two Evolve EM-CCD cameras (Photometrics, Huntington Beach, CA, USA). Image stacks of 2 µm were reconstructed in Deltavision softWoRx 6.1.1 software with a Wiener filter of 0.01 using channel-specific optical transfer functions[62]. Captured synapses were analyzed using Colocalize Spots MATLAB function on IMARIS. A synapse was counted if the distance between the center point of a presynaptic and postsynaptic puncta was equal to or less than the radius of the presynapatic puncta + 0.1 µm, an empirically determined scaling factor[63]. All experiments were analyzed blind to groups.

RNA-seq analysis

Transcriptomics data of spinal cord from naive mice and SNI-injured mice was taken from Gene Expression Omnibus accession GSE111216[26]. In short, RNA-Seq data have been trimmed with Trimmomatic v0.32[64], then mapped on UCSC's mouse genome version mm10 grabbed from ftp://ussd-ftp.illumina.com/Mus_musculus/UCSC/mm10/ using tophat v2.0.11[65] and bowtie v1.0.0[66]. Differential gene expression detected at gene level from experimental triplicates using cuffdiff v2.2.1[67].

RNAscope

The RNAscope Fluorescent Multiplex Assay (ACD Biosystems) was performed according to the ACD protocol for fresh-frozen tissue. Perfusion fixed spinal cords from animals at multiple time-points after injury were sectioned at 10 µm on a cryostat and hybridized with C1qa mRNA probe (ACD cat#: 441221). The ACD 3-plex served as a negative control and applied on one section per slide to confirm signal specificity. The probes were amplified according to the manufacturer's instructions and labeled with Alexa 488 nm fluorophores. For RNAscope analysis, the entire medial and central portions of LII of the dorsal horn was imaged and quantified at 40x magnification. Briefly,

RNAscope puncta above a brightness threshold were marked following a background subtraction in imageJ. ROIs were manually drawn on the DAPI, Gad2$^+$, or Tac1$^+$ channels to identify each individual cell that had at least 1 C1qa mRNA probe signal colocalized with the DAPI signal. The number of C1qa mRNA associated puncta was quantified in C1qa$^+$ cells using ImageJ. Cells that had no C1qa mRNA signal were excluded from the quantification.

Procedures for euthanasia

All animals prepared for immunohistochemistry or RNAscope were euthanized by intracardiac perfusion with histological fixatives under deep anesthesia. In the context of mice colony management, or complications occurring during surgeries, drug administration, behavior testing, or any animals reaching the humane endpoints described under McGill's animal protocols, the euthanasia methods of choice was cervical dislocation under isoflurane anesthesia.

Experimental design, statistics, and reproducibility

Sample sizes were determined based on pilot studies. In the absence of sex-specific differences, data from male and female animals were pooled. All experiments were conducted in a blinded manner, with random assignment of treatment groups and randomization of the testing order. Both pharmacology experiments were replicated in independent cohorts to confirm reproducibility. One baseline data point was excluded from the ANX M1.21 behavioral experiment due to an abnormally high value inconsistent with baseline measurements.

All statistical analyses were performed using GraphPad Prism (version 8, Windows). Only parametric tests were used, including one-way ANOVA, two-way ANOVA, and two-way repeated measures ANOVA, followed by Bonferroni's multiple comparisons test. For comparisons between two groups, unpaired or paired two-tailed t-tests were applied. All p-values and statistical tests are reported in the results and figure legends.

Reporting summary

Further information on research design is available in the Nature Portfolio Reporting Summary linked to this article.

Data availability

Transcriptomics data analysis in Fig. 1a is performed on a previously generated data deposited in the Gene Expression Omnibus under the accession GSE111216[26]. The single-cell RNA-sequencing analysis in Supplementary Fig. 3a is performed on a previously generated data deposited in the Gene Expression Omnibus under the accession GSE162807[27]. Source data are provided with this paper.

References

1. Costigan, M., Scholz, J. & Woolf, C. J. Neuropathic pain: a maladaptive response of the nervous system to damage. *Annu Rev. Neurosci.* **32**, 1–32 (2009).
2. Baron, R., Binder, A. & Wasner, G. Neuropathic pain: diagnosis, pathophysiological mechanisms, and treatment. *Lancet Neurol.* **9**, 807–819 (2010).
3. Inoue, K. & Tsuda, M. Microglia in neuropathic pain: cellular and molecular mechanisms and therapeutic potential. *Nat. Rev. Neurosci.* **19**, 138–152 (2018).
4. Chen, G., Zhang, Y.-Q., Qadri, Y. J., Serhan, C. N. & Ji, R.-R. Microglia in pain: detrimental and protective roles in pathogenesis and resolution of pain. *Neuron* **100**, 1292–1311 (2018).
5. Gilmore, S. A. & Skinner, R. D. Intraspinal non-neuronal cellular responses to peripheral nerve injury. *Anat. Rec.* **194**, 369–387 (1979).
6. Coull, J. A. et al. BDNF from microglia causes the shift in neuronal anion gradient underlying neuropathic pain. *Nature* **438**, 1017–1021 (2005).
7. Echeverry, S. et al. Spinal microglia are required for long-term maintenance of neuropathic pain. *Pain* **158**, 1792–1801 (2017).
8. Jeong, H. et al. High-resolution transcriptome analysis reveals neuropathic pain gene-expression signatures in spinal microglia after nerve injury. *Pain* **157**, 964–976 (2016).
9. Yousefpour, N. et al. Time-dependent and selective microglia-mediated removal of spinal synapses in neuropathic pain. *Cell Rep.* **42**, 112010 (2023).
10. Kuner, R. & Flor, H. Structural plasticity and reorganisation in chronic pain. *Nat. Rev. Neurosci.* **18**, 113 (2017).
11. Lorenzo, L. E. et al. Enhancing neuronal chloride extrusion rescues alpha2/alpha3 GABAA-mediated analgesia in neuropathic pain. *Nat. Commun.* **11**, 869 (2020).
12. Neniskyte, U. & Gross, C. T. Errant gardeners: glial-cell-dependent synaptic pruning and neurodevelopmental disorders. *Nat. Rev. Neurosci.* **18**, 658–670 (2017).
13. Schafer, D. P. et al. Microglia sculpt postnatal neural circuits in an activity and complement-dependent manner. *Neuron* **74**, 691–705 (2012).
14. Paolicelli, R. C. et al. Synaptic pruning by microglia is necessary for normal brain development. *Science* **333**, 1456–1458 (2011).
15. Gunner, G. et al. Sensory lesioning induces microglial synapse elimination via ADAM10 and fractalkine signaling. *Nat. Neurosci.* **22**, 1075–1088 (2019).
16. Hong, S. et al. Complement and microglia mediate early synapse loss in Alzheimer mouse models. *Science* **352**, 712–716 (2016).
17. Lui, H. et al. Progranulin Deficiency Promotes Circuit-Specific Synaptic Pruning by Microglia via Complement Activation. *Cell* **165**, 921–935 (2016).
18. Clark, A. K. & Malcangio, M. Fractalkine/CX3CR1 signaling during neuropathic pain. *Front Cell Neurosci.* **8**, 121 (2014).
19. Griffin, R. S. et al. Complement Induction in Spinal Cord Microglia Results in Anaphylatoxin C5a-Mediated Pain Hypersensitivity. *J. Neurosci.* **27**, 8699–8708 (2007).
20. Dickie, A. C. et al. Morphological and functional properties distinguish the substance P and gastrin-releasing peptide subsets of excitatory interneuron in the spinal cord dorsal horn. *Pain* **160**, 442 (2019).
21. Peirs, C. & Seal, R. P. Neural circuits for pain: Recent advances and current views. *Science* **354**, 578–584 (2016).
22. Cameron, D. et al. The organisation of spinoparabrachial neurons in the mouse. *Pain* **156**, 2061–2071 (2015).
23. Todd, A. J. Neuronal circuitry for pain processing in the dorsal horn. *Nat. Rev. Neurosci.* **11**, 823–836 (2010).
24. Ribeiro-da-Silva, A. in *The Rat Nervous System* (ed G. Paxinos) Ch. 7, 97-114 (Elsevier Academic Press, 2015).
25. Tsuda, M. Microglia in the spinal cord and neuropathic pain. *J. Diab. Investig.* **7**, 17–26 (2016).
26. Parisien, M. et al. Genetic pathway analysis reveals a major role for extracellular matrix organization in inflammatory and neuropathic pain. *Pain* **160**, 932–944 (2019).
27. Tansley, S. et al. Single-cell RNA sequencing reveals time- and sex-specific responses of mouse spinal cord microglia to peripheral nerve injury and links ApoE to chronic pain. *Nat. Commun.* **13**, 843 (2022).
28. Presumey, J., Bialas, A. R. & Carroll, M. C. Complement System in Neural Synapse Elimination in Development and Disease. *Adv. Immunol.* **135**, 53–79 (2017).
29. Stephan, A. H. et al. A dramatic increase of C1q protein in the CNS during normal aging. *J. Neurosci.* **33**, 13460–13474 (2013).
30. Bialas, A. R. & Stevens, B. TGF-beta signaling regulates neuronal C1q expression and developmental synaptic refinement. *Nat. Neurosci.* **16**, 1773–1782 (2013).
31. Stevens, B. et al. The classical complement cascade mediates CNS synapse elimination. *Cell* **131**, 1164–1178 (2007).

32. Gyorffy, B. A. et al. Local apoptotic-like mechanisms underlie complement-mediated synaptic pruning. *Proc. Natl Acad. Sci. USA* **115**, 6303–6308 (2018).
33. Yilmaz, M. et al. Overexpression of schizophrenia susceptibility factor human complement C4A promotes excessive synaptic loss and behavioral changes in mice. *Nat. Neurosci.* **24**, 214–224 (2021).
34. Sekar, A. et al. Schizophrenia risk from complex variation of complement component 4. *Nature* **530**, 177–183 (2016).
35. Ali, I., Chugh, D. & Ekdahl, C. T. Role of fractalkine-CX3CR1 pathway in seizure-induced microglial activation, neurodegeneration, and neuroblast production in the adult rat brain. *Neurobiol. Dis.* **74**, 194–203 (2015).
36. Sheridan, G. K. & Murphy, K. J. Neuron-glia crosstalk in health and disease: fractalkine and CX3CR1 take centre stage. *Open Biol.* **3**, 130181 (2013).
37. Fong, A. M., Alam, S. M., Imai, T., Haribabu, B. & Patel, D. D. CX3CR1 tyrosine sulfation enhances fractalkine-induced cell adhesion. *J. Biol. Chem.* **277**, 19418–19423 (2002).
38. Barragan-Iglesias, P. et al. Role of spinal P2Y6 and P2Y11 receptors in neuropathic pain in rats: possible involvement of glial cells. *Mol. Pain.* **10**, 29 (2014).
39. Maeda, M., Tsuda, M., Tozaki-Saitoh, H., Inoue, K. & Kiyama, H. Nerve injury-activated microglia engulf myelinated axons in a P2Y12 signaling-dependent manner in the dorsal horn. *Glia* **58**, 1838–1846 (2010).
40. Batti, L. et al. TMEM16F Regulates Spinal Microglial Function in Neuropathic Pain States. *Cell Rep.* **15**, 2608–2615 (2016).
41. Sipe, G. O. et al. Microglial P2Y12 is necessary for synaptic plasticity in mouse visual cortex. *Nat. Commun.* **7**, 10905 (2016).
42. Koizumi, S. et al. UDP acting at P2Y6 receptors is a mediator of microglial phagocytosis. *Nature* **446**, 1091–1095 (2007).
43. Simonetti, M. et al. Nuclear calcium signaling in spinal neurons drives a genomic program required for persistent inflammatory pain. *Neuron* **77**, 43–57 (2013).
44. Yu, Y. P., Gong, N., Kweon, T. D., Vo, B. & Luo, Z. D. Gabapentin prevents synaptogenesis between sensory and spinal cord neurons induced by thrombospondin-4 acting on pre-synaptic Cav alpha2 delta1 subunits and involving T-type Ca(2+) channels. *Br. J. Pharm.* **175**, 2348–2361 (2018).
45. Tau, G. Z. & Peterson, B. S. Normal development of brain circuits. *Neuropsychopharmacology* **35**, 147–168 (2010).
46. Coull, J. A. et al. Trans-synaptic shift in anion gradient in spinal lamina I neurons as a mechanism of neuropathic pain. *Nature* **424**, 938–942 (2003).
47. Kaila, K., Price, T. J., Payne, J. A., Puskarjov, M. & Voipio, J. Cation-chloride cotransporters in neuronal development, plasticity and disease. *Nat. Rev. Neurosci.* **15**, 637–654 (2014).
48. Inquimbert, P. et al. NMDA Receptor Activation Underlies the Loss of Spinal Dorsal Horn Neurons and the Transition to Persistent Pain after Peripheral Nerve Injury. *Cell Rep.* **23**, 2678–2689 (2018).
49. Lee, K. Y., Ratte, S. & Prescott, S. A. Excitatory neurons are more disinhibited than inhibitory neurons by chloride dysregulation in the spinal dorsal horn. *Elife* **8** (2019). https://doi.org/10.7554/eLife.49753.
50. Scott-Hewitt, N. et al. Local externalization of phosphatidylserine mediates developmental synaptic pruning by microglia. *EMBO J.* **39**, e105380 (2020).
51. Latremoliere, A. & Woolf, C. J. Central sensitization: a generator of pain hypersensitivity by central neural plasticity. *J. Pain.* **10**, 895–926 (2009).
52. Sorge, R. E. et al. Spinal cord Toll-like receptor 4 mediates inflammatory and neuropathic hypersensitivity in male but not female mice. *J. Neurosci.* **31**, 15450–15454 (2011).
53. Sorge, R. E. et al. Different immune cells mediate mechanical pain hypersensitivity in male and female mice. *Nat. Neurosci.* **18**, 1081–1083 (2015).
54. Taves, S. et al. Spinal inhibition of p38 MAP kinase reduces inflammatory and neuropathic pain in male but not female mice: Sex-dependent microglial signaling in the spinal cord. *Brain Behav. Immun.* **55**, 70–81 (2016).
55. Donovan, L. J. et al. Repopulated spinal cord microglia exhibit a unique transcriptome and contribute to pain resolution. *Cell Rep.* **43**, 113683 (2024).
56. Kohno, K. et al. A spinal microglia population involved in remitting and relapsing neuropathic pain. *Science* **376**, 86–90 (2022).
57. Zhou, L. J. et al. Microglia Are Indispensable for Synaptic Plasticity in the Spinal Dorsal Horn and Chronic Pain. *Cell Rep.* **27**, 3844–3859 e3846 (2019).
58. Chaplan, S. R., Bach, F. W., Pogrel, J. W., Chung, J. M. & Yaksh, T. L. Quantitative assessment of tactile allodynia evoked by unilateral ligation of the fifth and sixth lumbar nerves in the rat. *J. Neurosci. Meth* **53**, 55–63 (1994).
59. Decosterd, I. & Woolf, C. J. Spared nerve injury: an animal model of persistent peripheral neuropathic pain. *Pain* **87**, 149–158 (2000).
60. Shields, S. D., Eckert, W. A. 3rd & Basbaum, A. I. Spared nerve injury model of neuropathic pain in the mouse: a behavioral and anatomic analysis. *J. Pain.* **4**, 465–470 (2003).
61. Schafer, D. P., Lehrman, E. K., Heller, C. T. & Stevens, B. An engulfment assay: a protocol to assess interactions between CNS phagocytes and neurons. *Jove-J. Vis Exp.* (2014). https://doi.org/10.3791/51482.
62. Gustafsson, M. G. et al. Three-dimensional resolution doubling in wide-field fluorescence microscopy by structured illumination. *Biophys. J.* **94**, 4957–4970 (2008).
63. Hong, S., Wilton, D. K., Stevens, B. & Richardson, D. S. Structured Illumination Microscopy for the Investigation of Synaptic Structure and Function. *Methods Mol. Biol.* **1538**, 155–167 (2017).
64. Bolger, A. M., Lohse, M. & Usadel, B. Trimmomatic: a flexible trimmer for Illumina sequence data. *Bioinformatics* **30**, 2114–2120 (2014).
65. Kim, D. et al. TopHat2: accurate alignment of transcriptomes in the presence of insertions, deletions and gene fusions. *Genome Biol.* **14**, R36 (2013).
66. Langmead, B., Trapnell, C., Pop, M. & Salzberg, S. L. Ultrafast and memory-efficient alignment of short DNA sequences to the human genome. *Genome Biol.* **10**, R25 (2009).
67. Trapnell, C. et al. Differential analysis of gene regulation at transcript resolution with RNA-seq. *Nat. Biotechnol.* **31**, 46–53 (2013).

Acknowledgements

This work was funded by Canadian Institutes of Health Research (CIHR) operating grant MOP 136903, and project grant PJT-166195 and Louise and Alan Edwards Foundation (LAEF) to ARS. YDK was supported by a Canada Research Chair in Chronic Pain and related Brain Disorders. We are thankful to Dr. Masha Prager-Khoutorsky and McGill University Life Science Complex ABIF for their technical support. We also thank Dr. Ji Zhang for kindly giving us the CX3CR1 KO mouse line.

Author contributions

N.Y. designed and planned the entire study with the help of S.T. and S.L.; N.Y. carried out the majority of the experiments, prepared the figures and wrote the manuscript. S.T. designed and performed behavior experiments. M.P. performed genetic data analysis. B.S., J.S.A., F.B.B. performed neuropathic pain surgeries. V.B., V.C.C., M.S.L., H.D., F.B.B., N.R.K.A. and K.L. assisted with the histology experiments. H.D., R.R. and M.-E.P. contributed meaningfully to the writing of the revised version of the manuscript. CW (Wang) performed a portion of engulfment and synapse quantifications. CW (Wong) assisted with transgenic mice colonies and proofread the manuscript. AK (Khoutorsky) supported the super-resolution microscopy, transgenic studies, and contributed to manuscript editing. AK (Kania) provided MrgD-tdTom and Lmx1b-tdTom

mouse lines and MCC provided C4KO line. V.M., Y.A.Z., and T.Y. contributed to the design and execution of the ANX M1.21 component of the study. Y.D.K. contributed to the overseeing of the project as a whole, to extensive discussions and critical assessment of manuscript. L.D. granted us access to previously generated transcriptomics and contributed significantly to this component of manuscript. P.S., A.K., and J.M. edited the manuscript. A.R.S. oversaw the project as a whole and edited the manuscript.

Competing interests

N.Y., V.M., Y.A.Z., N.R.K.A., and T.Y. are employees of Annexon Inc., a venture-funded private biotechnology company. All other authors have no competing interests.

Additional information

Supplementary information The online version contains supplementary material available at https://doi.org/10.1038/s41467-025-59849-1.

Correspondence and requests for materials should be addressed to Alfredo Ribeiro-da-Silva.

Peer review information *Nature Communications* thanks the anonymous reviewers for their contribution to the peer review of this work. A peer review file is available.

[1]Dept. of Pharmacology and Therapeutics, McGill University, Montréal, QC, Canada. [2]Alan Edwards Centre for Research on Pain, McGill University, Montréal, QC, Canada. [3]Annexon Biosciences, Brisbane, CA, USA. [4]Dept. of Psychology, McGill University, Montréal, QC, Canada. [5]Dept. of Anesthesia, McGill University, Montréal, QC, Canada. [6]Montreal Neurological Institute, Dept. of Neurology and Neurosurgery, McGill University, Montréal, QC, Canada. [7]Department of Physiology, McGill University, Montréal, QC, Canada. [8]Faculty of Dental Medicine and Oral Health Sciences, McGill University, Montréal, QC, Canada. [9]Institut de recherches cliniques de Montréal (IRCM), Montréal, Québec, Canada. [10]Dept. of Anatomy and Cell Biology, McGill University, Montréal, QC, Canada. [11]Dép. de biochimie, microbiologie et bioinformatique, Université Laval, Québec, QC, Canada. [12]CERVO Brain Research Centre, Québec, QC, Canada. [13]Harvard Medical School and Boston Children's Hospital, Boston, MA, USA. [14]Division of Experimental Medicine, Faculty of Medicine and Health Science, McGill University, Montréal, QC, Canada. [15]Dép. de psychiatrie et neurosciences, Université Laval, Québec, QC, Canada.
✉e-mail: alfredo.ribeirodasilva@mcgill.ca